Spring 2018

Lyapunov stability analysis of switched microgrid systems

Bokang Zhou

Department:

LYAPUNOV STABILITY ANALYSIS OF SWITCHED MICROGRID SYSTEMS

by

BOKANG ZHOU

A THESIS

Presented to the Graduate Faculty of the

MISSOURI UNIVERSITY OF SCIENCE AND TECHNOLOGY

In Partial Fulfillment of the Requirements for the Degree

MASTER OF SCIENCE

in

ELECTRICAL ENGINEERING

2018

Approved by

Jonathan W. Kimball, Advisor
Mehdi Ferdowsi
Bruce McMillin

ABSTRACT

In this thesis, a Lyapunov-based method for analyzing the stability of a switched microgrid system is proposed. First, a small second-order system is explored as example to demonstrate the effectiveness of switching patterns on the stability of a system switching among different respectively stable operating points. Lyapunov function is employed in order to determine the proper state-based switching conditions under which global stability is guaranteed, or under which the system is driven unstable. Then, a linearized state-space model of a looped seven-node microgrid is established. Solid-state transformers (SSTs), distributed energy storage devices and synchronous generators are introduced and modeled in this system. The model uses accurate SST models to highlight the different performance in terms of stability between traditional power grid system and distributed microgrid system. Also, a control method is employed to ensure static stability. Based on this model, the system transfer matrix is derived and used in the Lyapunov function computation numerically. Finally, a high order system switching function is derived. The switching function is a state-based hypersurface. System stability may be ensured by switching the load or power command when the operating point cross the switching function. Conversely, system instability may be ensured with a different switching function. Finally, the approach is verified using MATLAB simulations.

ACKNOWLEDGMENTS

I am extremely thankful to my advisor Dr. Jonathan W. Kimball for his constant guidance and support throughout. He has always been willing to spend time giving me instructions and guides during his busy schedule. He always helps me patiently and provides useful suggestions when I meet with difficulties. I feel myself very lucky to be working with such a kind and decent advisor like him. He also impacts me so much mentally and makes me obtain a lot about how to cooperate with others and the responsibility I need to take. I am also grateful to Dr. Bruce McMillin and Dr. Mehdi Ferdowsi for being on my committee, and thanks for their good ideas in the discussion and academic help.

I also want to thank Dr. Isaac Leonard in Florida State University for his help. And I would also like to thank Jacob A. Mueller, Tamal Paul and William St. Pierre for their contribution to the ideas and advice. I also feel grateful to my parents and friends who have given me a lot of inspiration and support.

TABLE OF CONTENTS

Page

LIST OF ILLUSTRATIONS

Figure Page

LIST OF TABLES

Table Page

SECTION

1. INTRODUCTION

1.1. MICROGRID

The modern power systems have been becoming more intelligent and more reliable. This profits from the proposed concept of microgrid. Microgrids promote the traditional electric power delivery network to smart-grid by introducing the distributed energy resources (DERs). A special feature of microgrid is the ability to operate in islanded mode which means the microgrid can supply power to local load without connecting to the main grid all the time. Supported by the local generation sources and distributed energy storage devices (DESDs), the microgrid can not only manage the loads of the local network but sell extra power to the main grid as well. Microgrids are providing such flexible power supply but, at the same time, also causing problems. The control scheme of islanded microgrid are open to be researched actively. Different from the traditional power grid, DERs mostly have DC voltage and exchange power with AC bus through controlled SSTs. These DERs have relative lower inertia. Together with synchronous generators which have higher inertia, the dynamics of the system come to be very interesting. There are, also, power electronics devices in the SSTs which can make the control scheme even more complicated.

1.2. LYAPUNOV-BASED METHOD

To better serve the local users and cooperate with the main grid, a stable performance of the microgrid is required. In the physical domain, one of the methods to analyze the stability problem is using Lyapunov functions. It is a well-developed tool to study a lot of complicated power systems, of cause also microgrids, stability problems. In terms of

linear system, Lyapunov function can transfer the system response to a scalar function. It can also be used to describe the operating mode. For a switched system switching among different stable operating points, Lyapunov-like function can be used to analyze the stability problems. Certainly, it can be used to address network domain. A well-designed model is thus needed to combine all the sub-system together and make the system analyzable by Lyapunov-based methods.

1.3. LITERATURE REVIEW

The research about the dynamic behavior analysis of the traditional power grid have been performing for decades and have had sufficient achievements. Because of the high inertia and relatively slow dynamic response, the "quasi-static model" is earlier used to perform dynamic analysis successfully but with limitations in terms of faster response introduced by some power electronic devices [7]. The occurrence of "Time-varying phasor" breaks the limitation and is used often to analyze these kind of phenomena [2]. However, as the modern grid is developing, more and more emerging electrical energy resources and energy storage devices are coming into the power system. In 2004, a new concept "microgrid" was proposed in [11]. It also brought out the islanded mode and its meaning of a microgrid. In the following years, the increasing number of distributed generators and power electronics devices are causing challenges. Then, a hierarchical control for application in microgrids is discussed, and control strategies about reserve provision of DERs, loads and RESRs were proposed in [21]. In the well distributed microgrid system, stability is crucial, as each microgrid must support its own load with high power quality and reliability. Because of the introduction of Solid State Transformers (SSTs) [8] [15], the DC loads, DERs and RESRs are connected to the AC buses through SSTs, in which case the dynamics of microgrids mentioned in [9] are becoming even more complicated. With load perturbations, the dynamics of microgrids may be modeled as switched systems which is discussed in [5]. These dynamics prospectively causes more difficult stability issues and

control problems. A general principle in switched system analysis is that the stability of the switched system is not guaranteed by the stability of individual modes, but instead must be analyzed at the system level.

One possibility is to use a common Lyapunov function [14], that is, a single function that is applicable to all switching modes and satisfies all of the conventional requirements for Lyapunov stability. Sometimes, a common Lyapunov function is not possible, but Lyapunov-like functions [13] may be found. Samples of a Lyapunov-like function at switching instants form a decreasing series. In a switched system where the individual modes have different stable operating points, a common Lyapunov function is not possible; a set of Lyapunov-like functions may be possible, but switching conditions are needed [13].

Analyzing a complete microgrid poses serious computational challenges. A good model is the key for fast and accurate analysis. The main goal is to analyze the dynamics of the system, so a small signal state-space model is appropriate to be built. In an NSF sponsored system - the Future Renewable Electric Energy Delivery and Management (FREEDM) [10] uses 7-node system which has a reasonable size for the balance between the complicatedness and calculability to help analyze some power management and control issues. A seven-node loop-type microgrid with five SST-connected loads and two diesel generators could have a model with about one hundred states. For the system only has SSTs, [19] gives an accurate model on which the model proposed in this thesis is based, and [22] also proposed some ideas about the inverter model. The control strategy is also addressed. In [3] and [12], a three-phase generator model is implemented in the computer simulation. The exciter model of the generator is described in [18]. The governor and other parts of model are precisely stated in [16]. But in the above models, there are not combination of SSTs and generators. Another paper proposed a survey [1] which mentions the system modeling of a microgrid but without detailed control strategy. The generator model of the generator is also too complicated which can affect the dynamics observation to the SSTs.

Therefore, the following section focuses on a smaller example system first, an open-loop boost converter with only two states. Not only is the computational burden reduced, but also graphical methods are easier to visualize. However, the methods used can be extended to n-dimensional space. This thesis will illustrate that a two-state, two-mode switched system, where each mode is linear and stable, may be driven to instability through the choice of switching conditions. Thus, the derivation of constraints on switching is necessary. Section 2.1 introduces a state-space model of the switched boost converter system. In Section 2.2, the nonlinear model is converted to a linearized switched system. Section 2.3 introduces the basic Lyapunov stability theory and importantly proposes a method for determining the state-based switching condition. In Section 2.4 the simulation results verify the method and more detailed observation is given. At last, the results are discussed.

The remainder of the thesis is organized as follows. The similar method used in the example system will be used to make the system converge faster which means better stability. Section 3.1 introduces a larger 7-node state-space model of the microgrid system. In Section 3.2, there is the method for determining the state-based switching condition. Then, in Section 3.3, the method implementation is given. Finally, we have the conclusion.

2. SWITCHING CONTROL METHOD IN THE EXAMPLE SYSTEM

2.1. STATE-SPACE MODELING

A switching power converter may be represented with a switched state-space model composed of several state space equations in the form of (2.1) for switching mode i.

$$\dot{x} = A_i x + B_i u \tag{2.1}$$

The boost converter system analyzed here is shown in Fig. 2.1. This is a second order system, so in (2.1), x is a vector with two elements of states, u is the vector with two external input elements as in (2.2), and $\dot{x}$ is the time derivative of the state vector.

$$x = \begin{bmatrix} i_L \\ V_C \end{bmatrix}, \quad u = V_{in} \tag{2.2}$$

The model will be derived assuming that the switching of the controlled transistor T in the boost converter is ideal and the voltage drop of the diode is zero. The boost converter has two independent working modes in continuous conduction situation [20]. One is switch 'ON' mode, and the other is switch 'OFF' mode.

During 'ON' mode, the switch is closed while the diode is open. The inductor is charged through V_{in}. There is no current flowing from V_{in} to the capacitor, and the capacitor is discharging through the load resistor. The equivalent circuit is just two separate loops. We obtain the differential equations from the current mode as (2.3) and (2.4).

$$\dot{x}_1 = \frac{-R_L}{L} x_1 + \frac{V_{in}}{L} \tag{2.3}$$

$$\dot{x}_2 = \frac{-1}{(R_C + R)C} x_2 \tag{2.4}$$

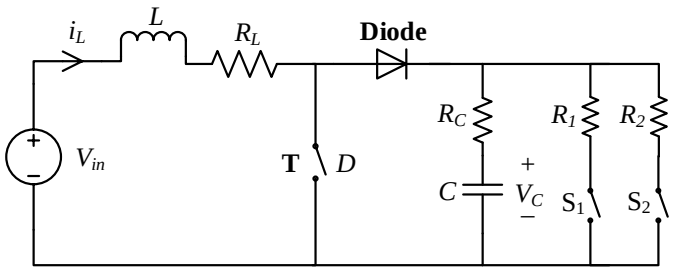

Figure 2.1. Actual circuit of the boost converter.

When the switch is OFF, the diode conducts, and the voltage source starts recharging the capacitor and providing voltage for the load. The system switches to a new mode with a set of differential equations defined in (2.5) and (2.6).

$$R_L x_1 + L\dot{x}_1 + R_C C\dot{x}_2 = V_{in} - x_2 \tag{2.5}$$

$$R(x_1 - C\dot{x}_2) = x_2 + R_C C\dot{x}_2 \tag{2.6}$$

With simple modification to the above equations, the state space equations to these two modes are represented in the equations (2.7) and (2.8)-(2.9) respectively.

$$A_{on} = \begin{bmatrix} \frac{-R_L}{L} & 0 \\ 0 & \frac{-1}{(R_C+R)C} \end{bmatrix},\ B_{on} = \begin{bmatrix} \frac{1}{L} \\ 0 \end{bmatrix} \tag{2.7}$$

$$A_{off} = \begin{bmatrix} -\frac{R_C R_L + R(R_C+R_L)}{L(R+R_C)} & \frac{-R}{L(R+R_C)} \\ \frac{R}{L(R+R_C)} & \frac{-1}{(R+R_C)C} \end{bmatrix} \tag{2.8}$$

$$B_{off} = \begin{bmatrix} \frac{1}{L} \\ 0 \end{bmatrix} \tag{2.9}$$

The duty ratio is not yet included, as the time spent in each switching state has not yet been addressed.

2.1.1. Average Model. Based on the two-mode model above, the average state space model [6] can be obtained with all the equations weighted by the time of contribution. This is given by the duty ratio D as shown in (2.10) and (2.11).

$$A_{av} = DA_{on} + (1 - D)A_{off} \tag{2.10}$$

$$B_{av} = DB_{on} + (1 - D)B_{off} \tag{2.11}$$

Substituting A_{on} and A_{off} into these two equations above yields the state-transition matrix (2.12) and (2.13) of the average model which can be used for later study.

$$A_{av} = \begin{bmatrix} -\frac{R_C R_L + R[(1-D)R_C + R_L]}{L(R+R_C)} & -\frac{(1-D)R}{L(R+R_C)} \\ \frac{(1-D)R}{L(R+R_C)} & -\frac{1}{(R+R_C)C} \end{bmatrix} \tag{2.12}$$

$$B_{av} = \begin{bmatrix} \frac{1}{L} \\ 0 \end{bmatrix} \tag{2.13}$$

The duty ratio D is now introduced in A_{av}. Therefore, the model is nonlinear [6].

2.1.2. Small Signal Model. A small signal model, compared to the large signal model, is a model linearized near a stable operating point. Linear models are easier to analyze because straightforward methods are available to find Lyapunov functions or otherwise determine stability. The linearized small signal model [17] is shown as (2.14) in which $\tilde{x}$ represents the deviation between the current state x and the steady state X as in (2.15).

$$\dot{\tilde{x}} = \tilde{A}_i \tilde{x} \tag{2.14}$$

$$\tilde{x} = x - X_i \tag{2.15}$$

In this system, the state transition matrix $\tilde{A}_i$ in the linearized model is the same as A_{av} in the average model. The system small signal model ends up to be (2.16).

$$\dot{\tilde{x}} = A_{av}\tilde{x} \tag{2.16}$$

2.2. DYNAMICS OF SWITCHED SYSTEM

A prototypical switched system [13] can be defined as

$$\dot{x} = f_p(x(t)), \quad p \in \mathcal{P} \tag{2.17}$$

$\mathcal{P}$ is an index set, and it is typically a subset of a finite-dimensional linear vector space. The fundamental dynamics of such a switched system occurs when switching actions are executed at discrete time instants. In Section 2.1,(2.14) is the linearization of (2.17) around steady state X_i while the system stays in mode i. When the system is switched from mode i to mode j at time instant t_s, the new small-signal state becomes (2.18) where $\Delta_s = X_j - X_i$ [17].

$$\begin{aligned} \tilde{x}(t_s^+) &= \tilde{x}(t_s^-) - \Delta_s \\ &= x_s - X_j \end{aligned} \tag{2.18}$$

That is, the actual state x does not change, but the small-signal state $\tilde{x}$ changes because there is a shift in the "origin" (the relevant steady-state operating point). In general, x may not be near enough to X_j to satisfy small-signal linearization assumptions, but for the boost converter analyzed below, the linearization is valid over a large region.

2.3. LYAPUNOV STABILITY ANALYSIS

Lyapunov stability is one of the methods that discuss the solutions of differential equations describing dynamical systems. The stability of the system can be determined by certain conditions of the Lyapunov function. The Lyapunov stability idea can be applied to high order systems which helps in this topic which involves a high order microgrid system.

2.3.1. Definition. For a switched system before any switching action to be asymptotically stable, the eigenvalues of the state transition matrix should have negative real parts. In the linear state space model form, the condition is equivalent to the following expression: There exists a positive definite symmetric matrix Q for which a unique positive definite symmetric matrix P satisfies the Lyapunov equation as (2.19).

$$A^T P + PA = -Q \tag{2.19}$$

The corresponding Lyapunov function is defined as (2.20).

$$V(\tilde{x}) = \tilde{x}^T P \tilde{x} \tag{2.20}$$

The derivative of V is given as

$$\dot{V}(\tilde{x}) = -\tilde{x}^T Q \tilde{x} \tag{2.21}$$

The Lyapunov function $V(\tilde{x})$ must be positive definite, radially unbounded and non-increasing for the system to be stable. This condition can be expressed as

$$V(\tilde{x}) > 0, \ \forall \ \tilde{x} \neq 0 \tag{2.22}$$

$$V(0) = 0 \tag{2.23}$$

$$\dot{V}(\tilde{x}) \leq 0 \tag{2.24}$$

For a switched linear system, it is natural to consider quadratic common Lyapunov functions, of the form (2.20), such that for some positive definite symmetric Q we have

$$A_p^T P + P A_p \preceq -Q, \ \forall p \in \mathcal{P}. \tag{2.25}$$

However, in the absence of a common Lyapunov function, multiple Lyapunov functions may be used.

2.3.2. Multiple Lyapunov Functions. For the boost converter system described in Section 2.1, it is not hard to prove that the system is locally asymptotically stable in any single mode (under a certain constant load), but the stability of the switched system cannot be determined using only the individual information of each mode. Switching actions could drive the system unstable. Here, a condition is derived whereby a switched system consisting of stable modes may be driven unstable by constrained switching [4].

Consider the switched system (2.17) with $\mathcal{P} = \{1, 2\}$. In terms of the linearized boost converter system, suppose that both systems

$$\dot{\tilde{x}}_1 = \tilde{A}_1 \tilde{x}_1, \quad \dot{\tilde{x}}_2 = \tilde{A}_2 \tilde{x}_2 \tag{2.26}$$

are asymptotically stable, and let V_1 and V_2 be their Lyapunov functions respectively as (2.27).

$$V_1(\tilde{x}) = \tilde{x}_1^T P_1 \tilde{x}_1, \ V_2(\tilde{x}) = \tilde{x}_2^T P_2 \tilde{x}_2 \tag{2.27}$$

Obviously, the stability depends on the switching signal σ, and V_σ is a piecewise-continuous Lyapunov-like function for this switched system [13] as shown in Fig. 2.2. The system is switched after enough dwell time each time so that the state is nearer to the corresponding stable operating point. Both V_1 and V_2 have a decreasing trend. In this case, the overall system is stable. On the contrary, the switched system would be unstable if

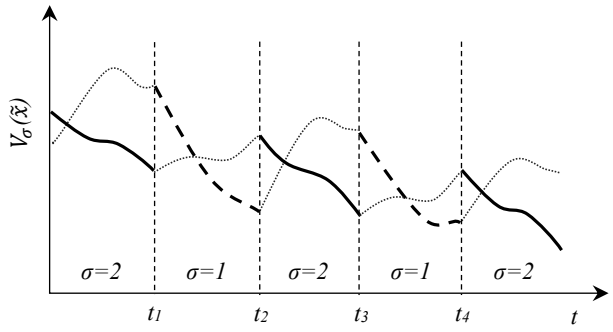

Figure 2.2. Switched system stability using multiple Lyapunov functions.

V_σ keeps increasing in general. Equivalently, the switched system will be unstable if the distance from x to the individual operating points grows without bound, or at the least enters a region where the linearization is no longer valid.

2.3.3. Switching Condition for Guaranteed Instability. There are two categories of switching control methods which are time-dependent switching and state-dependent switching. For the boost converter, time-dependent switching was found to be stable across a wide range of rates, so state-dependent switching is used here instead.

The switching condition here is derived by using trajectory analysis. As mentioned in last subsection, $\dot{V}_p(\tilde{x}) \leq 0$ is one of the conditions that assure the system stability with respect to one certain mode. This condition can also help obtain the inter-mode switching. The system will become unstable if $\dot{V}_p(\tilde{x}) \geq 0$. Within one mode, this cannot happen because each mode is independently asymptotically stable. However, by monitoring the changing trend of V_p of the target mode to which the system will switch, there may be a condition for which $\dot{V}_p(\tilde{x}) = 0$ or even $\dot{V}_p(\tilde{x}) > 0$.

Consider Fig. 2.3. The system is switching between mode 1 and mode 2. Each mode corresponds to a different constant load, and the stable operating points are X_1 and X_2 respectively. Let the system initially be in mode 2. The corresponding small-signal states

are $\tilde{x}_2 = x - X_2$. We are now only interested in the changing trend of $V_1 = \tilde{x}_1^T P_1 \tilde{x}_1$ with respect to mode 2. If the switching occurs at the correct moment, V_1 will have grown to its maximum value while in mode 2.

This condition is “worst-case switching". In Fig. 2.3, $V_1(\tilde{x}) = c_1$ and $V_2(\tilde{x}) = c_2$ are level sets for mode 1 and mode 2 respectively at the state point of x. For convenience in the illustration, we use vectors $\boldsymbol{l_1}$ and $\boldsymbol{l_2}$ to indicate $\tilde{A}_1\tilde{x}_1$ and $\tilde{A}_2\tilde{x}_2$ respectively, with $\boldsymbol{l_1}$ and $\boldsymbol{l_2}$ representing the moving direction of the states in mode 1 and mode 2 respectively. While in mode 2, as the state values varying, vector $\boldsymbol{l_2}$ could point either outwards or inwards, i.e., it forms an angle greater than or less than 90° respectively with the line connecting to the new origin, X_1. If it points inwards, the state will approach X_1. If it points outwards, the state will move away from X_1 until vector $\boldsymbol{l_2}$ becomes perpendicular to the line going through the current state x and the point X_1. A complementary switching law may be found while in mode 1 and switching to mode 2.

Mathematical conditions may be derived from the Lyapunov functions and state dynamics as follows.

$$\textit{From mode 2 to mode 1 when: } \left.\frac{\mathrm{d}V_1}{\mathrm{d}t}\right|_{\tilde{x}=x-X_2} = 0 \tag{2.28}$$

$$\Rightarrow \frac{\partial V_1}{\partial \tilde{x}_2} \cdot \frac{\mathrm{d}\tilde{x}_2}{\mathrm{d}t} = 0 \tag{2.29}$$

$$\Rightarrow [(P_1 + P_1^T) \cdot \tilde{x}_2 + (P_1 + P_1^T) \cdot \Delta_s] \cdot (A_2 \cdot \tilde{x}_2) = 0 \tag{2.30}$$

$$\Rightarrow [(P_1 + P_1^T) \cdot \tilde{x}_1] \cdot (A_2 \cdot \tilde{x}_2) = 0 \tag{2.31}$$

Switching then proceeds autonomously, but in a manner constrained by the state trajectories [13].

2.3.4. Switching Condition for Guaranteed Stability. Similarly, the same concept can be applied to guarantee the system stability by modifying the switching condition from “worst-case switching" to “best-case switching". The method for determining the

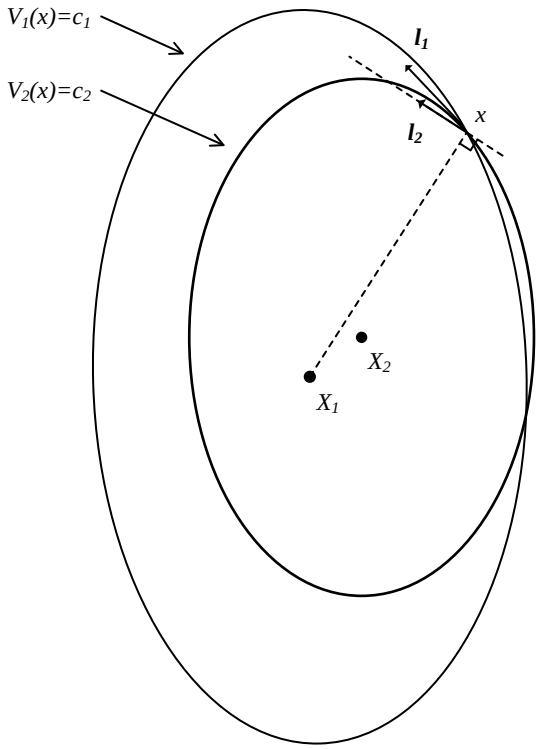

Figure 2.3. State-dependent switching condition.

switching point is totally the same as mentioned in subsection 2.3.3, but only the direction of hitting the switching curve is right opposite. By doing this, the system will be going toward a more damping situation upon every switching and force the system converging faster.

The simulation has been done to demonstrate the effectiveness of the switching control method in both of these two cases.

2.4. SIMULATION AND RESULTS

To demonstrate the effectiveness of the switching strategy, a Simulink model was built to plot the trajectories of the states with the state-dependent switching surfaces applied. The linearized state space model of the boost converter derived in Section II was used as

Table 2.1. Simulated system parameters.

Parameter	**Value**
Duty Ratio (D)	D
Inductance (L)	0.95 mH
Capacitance (C)	120 μF
Resistance C (R_C)	0.01 Ω
Resistance L (R_L)	0.01 Ω
Input Voltage (V_{in})	200 V
Resistance Load (R)	R_σ

Table 2.2. Loads and duty ratios.

Sequence	**Value** R_1	**Value** R_2	**Value** D
1	500 Ω	30 Ω	0.5
2	100 Ω	10 Ω	0.5

a study objective. The system simulation is operated base on the parameters shown in the following tables. The system parameters are given in Table 2.1, and the two modes in the simulation are shown in Table 2.2.

Along with the Simulink simulation, all the switching surfaces curves are calculated in Mathematica. The simulation is divided into two parts. In the first part, three simulations are performed under the duty ratio of 0.5 but three different load sets. This identifies the instabilities of the system when differing among the various stable loads. In the second part, the duty ratio is reduced to 0.1, and the load changed also. This is to check the effect of duty ratio to the system instability. Due to the real characteristics of the practical system, it is not necessary for the states to go to infinity. Once the inductance current and capacitor voltage both go negative, the boost converter will no longer be functional and the linearization assumptions will fail. Since the capacitor voltage limit is the most fragile one to keep that almost no negative capacitor voltage can be accepted, we can assume the stability condition as the following where I_m is the maximum current value the system can handle and V_{ms} is

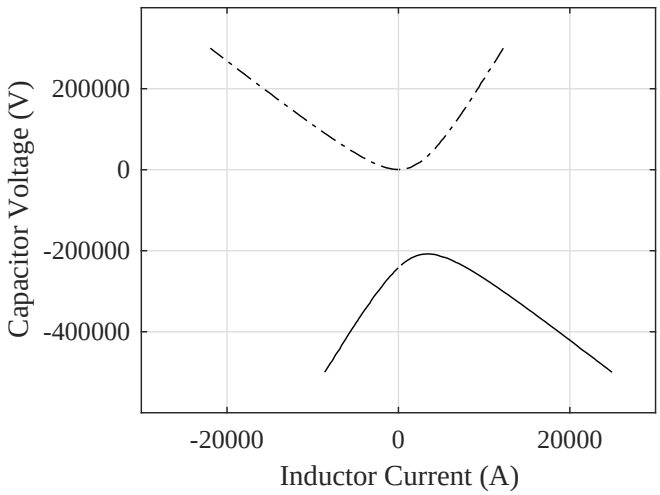

Figure 2.4. Hyperbola switching surface - Simulation I.

the maximum stable state voltage.

$$I \in [-I_m, I_m] \quad and \quad V \in (0, 2V_{ms}) \tag{2.32}$$

Negative current is possible with synchronous rectification.

2.4.1. Simulation I: Instability (Light Loads). The ideal output voltage is $V_o = \frac{V_{in}}{1-D}$, which is $400\,V$. In the first simulation, the initial condition of the system state is $I = 20\,A$, $V = 390\,V$.

One switching surface is an ellipse and the other is the upper branch of the hyperbola shown in Fig. 2.4. One is for switching from mode 2 to mode 1, and the other one is for switching from mode 1 back to mode 2.

The two curves are pretty close to each other around the two stable points that they are almost collinear. As shown in Fig. 2.5, the two black points identify the two steady state points. That two curves are the switching surfaces. In detail, after starting from an initial state point, the trajectory keep going anticlockwise. If the system is in mode 2, the system switch happens only when the trajectory hits the red dashed line upwards; On the contrary, if the system is in mode 2, it switches when the path hits the solid green line from the top.

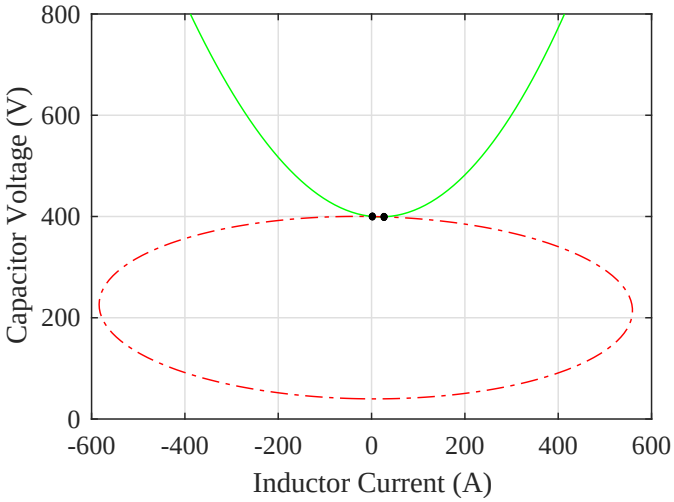

Figure 2.5. Normal scale - Simulation I.

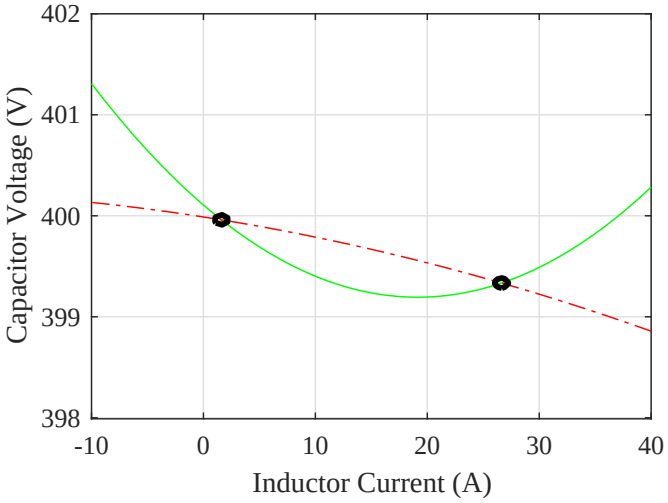

Figure 2.6. Zoomed in - Simulation I.

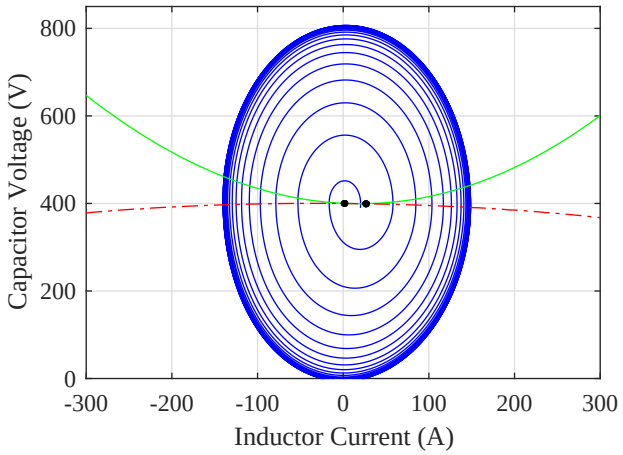

Figure 2.7. System trajectory for Simulation I.

The red curve and the green curve are intersected right at X_1 and X_2 (Fig. 2.6) which means no matter how close the initial states are to any one of the stable points, the trajectory may still be able to hit the switching curve, and the system goes unstable.

With this in mind, we set the initial point a little further. Back to the result in Fig. 2.7, the trajectory shows that the oscillation of the system is huge then the inductance current easily becomes negative, but we can still accept it. It is also shown in the trajectory that the capacitor voltage finally crosses the zero line which means the system is finally driven unstable successfully even the trajectory ends up in a limit cycle instead of going far away to infinity.

2.4.2. Simulation II: Instability (Heavier Loads). This time the system load changed to be a little heavier than in the first simulation. The initial point is the same as before. The difference is that the upper switching curve is calculated to be a parabola like Fig. 2.8.

The lower curve is still an ellipse. As the trajectory shown in Fig. 2.11, the system again is unstable. Fig. 2.9 and Fig. 2.10 show the detail of the switching map shape.

Additional load conditions fall into one of these two categories, or a third category in which the parabolic surface becomes an ellipse.

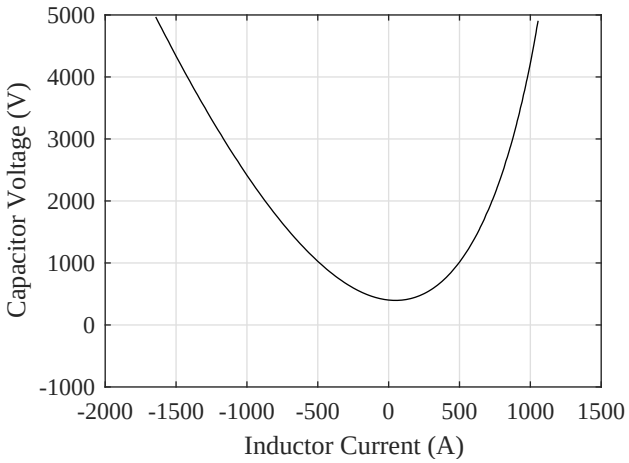

Figure 2.8. Parabola switching surface - Simulation II.

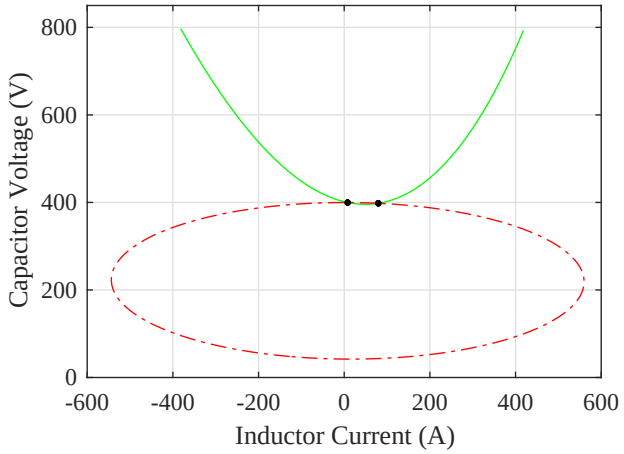

Figure 2.9. Normal scale - Simulation II.

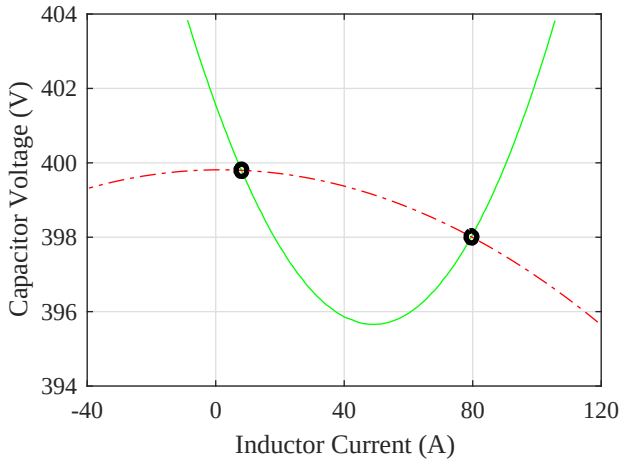

Figure 2.10. Zoomed in - Simulation II.

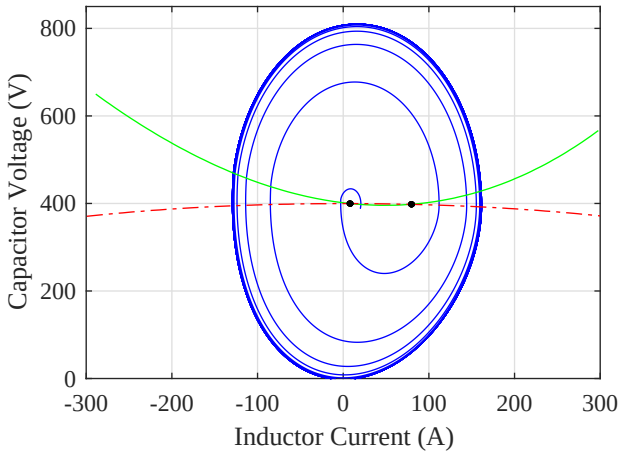

Figure 2.11. System trajectory for Simulation II.

2.4.3. Simulation III: Stability. In this case, the switching flags are modified to make the switching only happens when the trajectory hit the switching curve from the opposite side to which in the cases before. Fig. 2.12 shows the case without switching control, so the system have poor damping and takes long time to settle down. Fig. 2.13 shows the case with the switching control, and the system damped much faster obviously. This can be better observed from Fig. 2.14 and Fig. 2.15. They shows the changing of the Lyapunov function V_s (blue solid line) and 2 states. As we can see, the Lyapunov function converged faster in the switching controlled case which is Fig. 2.15 than that in the case without control in Fig. 2.14. According to the result, the system can be driven more stable by using state-based switching control.

The next step will be to derive conditions that guarantee stability for the microgrid system which is surly much larger. To guarantee stability, in a sense, may be seen as the dual problem: what are the switching conditions so that the Lyapunov-like function is guaranteed to decrease?

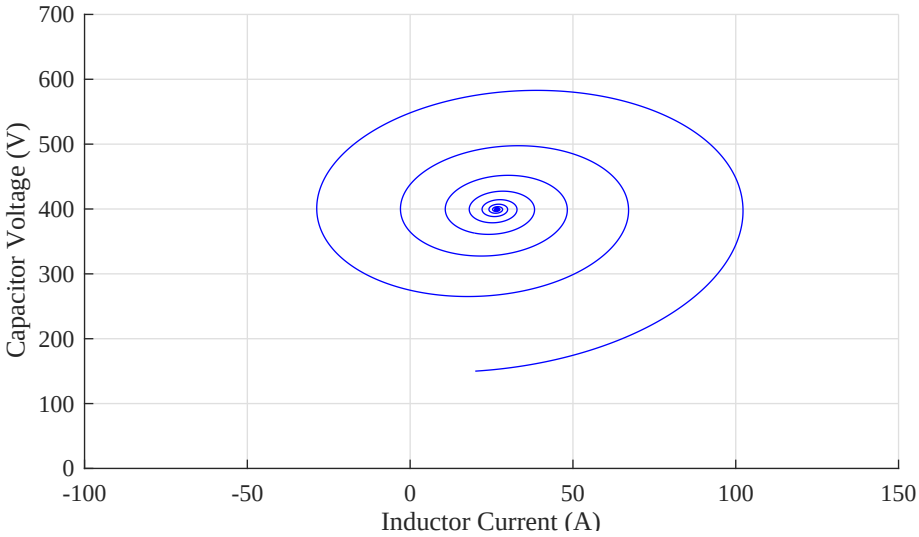

Figure 2.12. System trajectory for Simulation III.

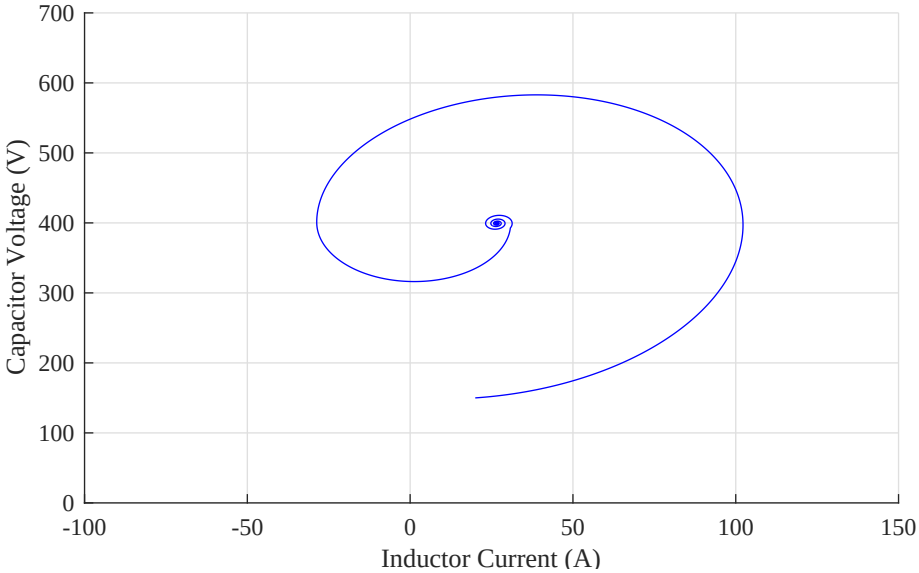

Figure 2.13. System trajectory for Simulation IV.

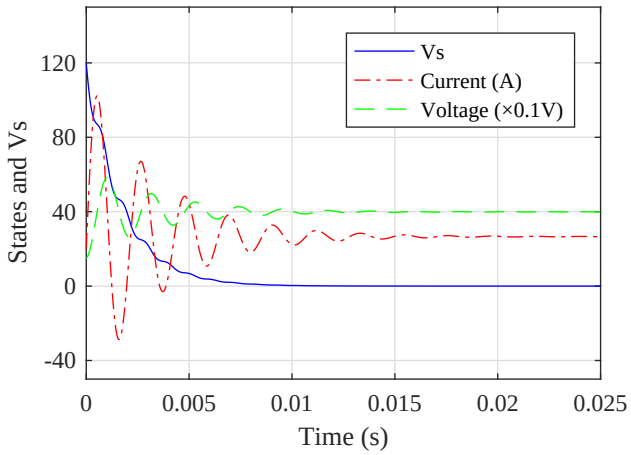

Figure 2.14. Switching controlled case.

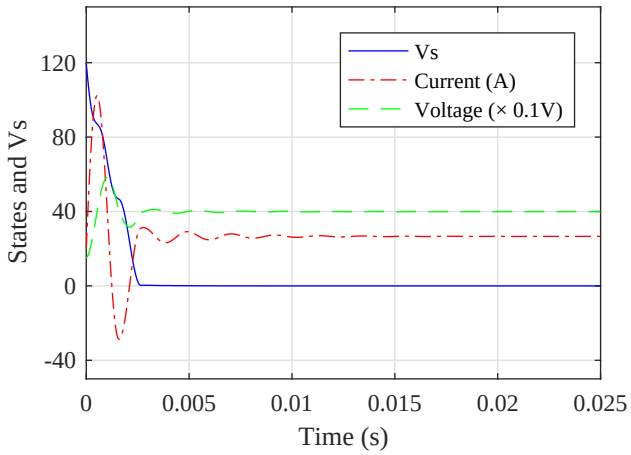

Figure 2.15. Without switching control.

2.5. SIMULATION RESULTS ANALYSIS

An open loop boost converter system is able to be destabilized by switching even if all individual subsystems are stable. The state-dependent worst-case switching strategy described in this paper works for driving a relatively uncomplicated boost converter system unstable. This method may be implemented on a larger dynamic system, such as a microgrid, at least to prove the possibility of the instability of such a system.

Between these two extremes lie switching conditions that result in bounded, but large, stable oscillations.

The shapes of the worst-case switching boundaries were observed to change from hyperbolas to parabolas to ellipses, depending on load and duty ratio. These differences may also illuminate the stability conditions.

3. OVERVIEW OF THE SEVEN-NODE MICROGRID SYSTEM

3.1. MICROGRID MODELING

The proposed microgrid system is an islanded, looped system as shown in Fig. 3.1. It consists of seven buses. Five of them are SST based DESD buses with constant impedance loads. The other two of them are diesel generators of witch one operating in droop mode and another operating in isochronous mode. Both generators have no load on the buses. The feeder is rated at 12.47 kV and the two generators are rated at 1.425 MVA and 380 V_{L-N} each. The transformers are rated at 1.5 MVA, 0.38 kV/12.47 kV. The transmission lines have a positive sequence resistance of 0.77 Ω, positive sequence inductance of 1.97 mH. The droop generator (G2) is set to run at 400 kW at 5% droop.

3.1.1. Park's Transformation. Park's transformation is often used in the three-phase power system to transfer three-phase voltages and currents from abc-axis based reference frame to dq-axis based reference frame. The transformation is shown below.

$$\begin{bmatrix} f_d \\ f_q \\ f_0 \end{bmatrix} = \frac{2}{3} \begin{bmatrix} \cos(\omega t) & \cos(\omega t - \frac{2\pi}{3}) & \cos(\omega t + \frac{2\pi}{3}) \\ -\sin(\omega t) & -\sin(\omega t - \frac{2\pi}{3}) & -\sin(\omega t + \frac{2\pi}{3}) \\ \frac{1}{2} & \frac{1}{2} & \frac{1}{2} \end{bmatrix} \begin{bmatrix} f_a \\ f_b \\ f_c \end{bmatrix} \tag{3.1}$$

If the system has three-phase equivalent currents and voltages, then there will be no zero components while calculating. For the convenience and consistency of the following work, dq reference frame will be used for all the system equations.

3.1.2. Diesel Generator Modeling. The traditional synchronous generator models differ a lot in the aspect of how accurately the generator features are expressed. The more major the generators playing as a role in the system, the more accurate the generator model need to be. Normally, a very large power system always have hundreds or thousands of

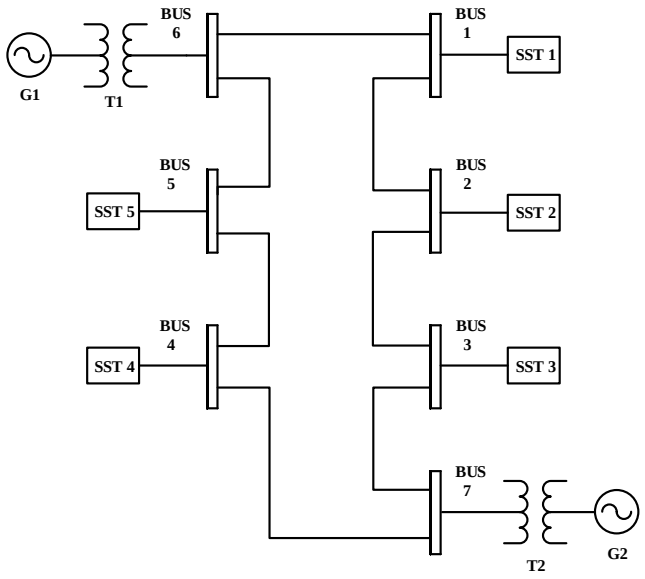

Figure 3.1. The microgrid system configuration.

power components so that the model will have also very high order which could become a disaster for calculation and analysis. For timely real time prediction and decision-making, we are more prone to use relatively simple model with only crucial feature kept and ignore those parameters which are not going to impact the main analysis work. In the seven-node system used here, the effects of the SSTs interest us more because the power electronic switching is involved witch can make the system dynamics even dramatic. As a result, the three-order practical synchronous generator model is employed in this thesis.

The three-order practical model is the simplest model while the excitation dynamics still needs to be considered. Some assumptions are made about this model: (1) Ignore the dynamics of the d, q windings of the stator; (2) In the stator voltage equations, the angular frequency always satisfies $\omega \approx \omega_n$ which is the nominal frequency; (3) Ignore the damping winding D and Q. The D and Q axis output currents for the isochronous generator in global

frame are

$$\begin{cases} \dot{i}_D = \dfrac{1}{L_g}(-R_g i_D + \omega i_Q L_g - \dfrac{v_{bD}}{T_{ratio}} + E_D) \\ \dot{i}_Q = \dfrac{1}{L_g}(-R_g i_Q - \omega i_D L_g - \dfrac{v_{bQ}}{T_{ratio}} + E_Q) \end{cases} \tag{3.2}$$

The terminal voltage equation is

$$u_t = \sqrt{(\frac{v_{bD}}{T_{ratio}})^2 + (\frac{v_{bQ}}{T_{ratio}})^2} \tag{3.3}$$

The generator transient electromotive force can be written in this form

$$E_q = \frac{\omega L_{af} E_f}{\sqrt{2} R_f} \tag{3.4}$$

The rotor equation of motion is modified to be

$$\dot{\omega} = \frac{\omega_n}{2H \cdot S_B}(P_m - P_e) \tag{3.5}$$

And another rotor equation of motion is

$$\dot{\delta} = \omega - \omega_s. \tag{3.6}$$

Here ω_s is the synchronous angular frequency of the system. It is, in other words, the frequency of the global reference frame relative to the static *abc* frame. For grid-connected systems, ω_s is the nominal grid frequency. In islanded systems, ω_s is the frequency of whichever subsystem chosen as the global reference frame.

3.1.2.1. Governor control. The governor here refers to the speed controller for the diesel engine. The engine needs to run at a preset speed to keep the generator producing required power constantly. The generator $G1$ that operates in isochronous mode must have the ability to produce sufficient power to supply loads together with other power sources and maintain the power balance of the whole microgrid. This process can be represented

by a PI controller. It is used to take the difference between the nominal frequency and the generator frequency to generate corresponding active power command.

$$\dot{\theta} = \omega_n - \omega \tag{3.7}$$

$$P_m = k_{im}\theta + k_{pm}\dot{\theta} \tag{3.8}$$

The electrical power produced by the generator can be represented by

$$P_e = E_Q i_Q + E_D i_D \tag{3.9}$$

Then, the rotor equation can be obtained. The generator $G2$ is designed to operate at droop mode. The engine is represented as $\frac{1}{R_P}$, the power command signal comes out through droop in terms of ω to get P_m. R_P and R_Q are the $P-\omega$ and $Q-V$ droop regulations for the droop generator $G2$ respectively.

$$P_m = T_n\omega_n + \omega_n\frac{1}{R_P}(\omega_n - \omega) \tag{3.10}$$

3.1.2.2. Excitation system. The excitation system is using an ideal fast exciter as below. The signals are already linearized, and the effect of field current and feedback excitation control are ignored. Also, to mostly simplify the exciter model, power system stabilizer is not used in the model.

$$\dot{V}_i = V_{ref} - V_t \tag{3.11}$$

The field voltage is set by PI controller.

$$\dot{E}_f = k_{pv}\dot{V}_i + k_{iv}V_i \tag{3.12}$$

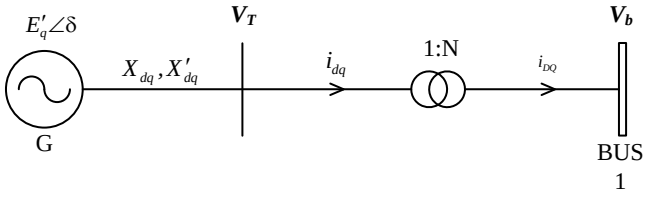

Figure 3.2. The generator and transformer configuration.

In $G2$, the desired line to line voltage E_q^* at the droop generator is introduced. E_q^* can be calculated from $Q-V$ droop equations. Then a PI controller is used to set the field voltage.

$$\dot{E}_i = E_q^* - E_q \tag{3.13}$$

$$\dot{E}_f = k_{pe}\dot{E}_i + k_{ie}E_i \tag{3.14}$$

$$\theta_q = \delta - \frac{\pi}{2} + \tan^{-1}(\frac{V_{bQ}}{V_{bD}}) \tag{3.15}$$

θ_q is the angle between the local voltage and global bus voltage. It is used in the E_q^* equation.

$$E_q^* = \frac{\omega L_g}{nV_t\cos\theta}(V_{ref} - V_t + R_Q Q_r) + \frac{V_t}{\cos\theta} \tag{3.16}$$

Q_r is the rated reactive power which is set by 0.

3.1.2.3. Transformer modeling. The transformer is represented by an ideal voltage step up device between the terminal of the generator and the bus, and it is an ideal transformer with the ratio of T_{ratio}=N:1=$12.47kV/0.380kV$. Other parameters like resistance, the negative and zero sequence components are all omitted. The structure is shown in Fig. 3.2.

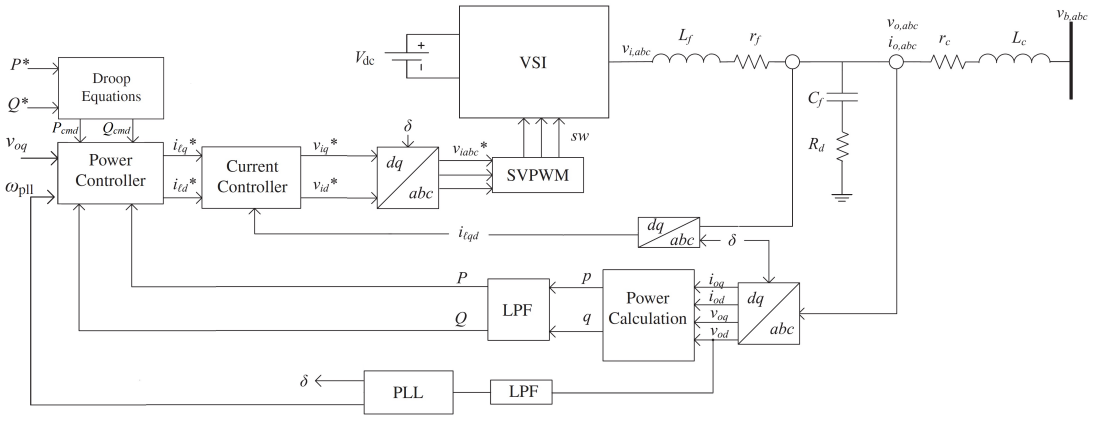

Figure 3.3. Inverter control diagram.

3.1.3. Inverter Modeling. The inverter dynamic model is based on the microgrid dynamic model from [19]. A detailed description of the structure and control of a SST based inverter will be given below. As mentioned in section 3.1.1, the state space equations of the system will be expressed in dq reference frame. To start with, the control diagram is shown as Fig. 3.3. Each inverter is connected to the bus through a LCL filter. A constant impedance load is connected to each bus. The input of the converter is the active power command and the reactive power command set by the operator according to the load requirement or scheduled plans. The converter will be operating in droop mode which requires a droop controller to set up the proper operating parameters.

3.1.3.1. Phase-locked loop (PLL). To obtain phase and frequency of the inverter, a traditional PLL is used. The PLL locks the q-axis to be in phase with the output voltage by forcing the d-axis voltage to be 0. So a proportional-integral (PI) controller is used here.

The PLL equations are

$$\dot{v}_{od,f} = \omega_{c,PLL} v_{od} - \omega_{c,PLL} v_{od,f} \tag{3.17}$$

$$\dot{\phi}_{PLL} = 0 - v_{od,f} \tag{3.18}$$

$$\omega_{PLL} = \omega_n + k_{i,PLL}\phi + k_{p,PLL}\dot{\phi} \tag{3.19}$$

$$\dot{\theta} = \omega_{PLL} \tag{3.20}$$

3.1.3.2. Outer control loop. The output current and voltage can be measured from the LCL filter. The active power p and reactive power q are calculated from these current and voltage and then pass through a low-pass filter before going to the droop controller. The power equations are

$$p = \frac{3}{2}(v_{od} i_{od} + v_{oq} i_{oq}) \tag{3.21}$$

$$q = \frac{3}{2}(v_{oq} i_{od} - v_{od} i_{oq}) \tag{3.22}$$

$$\dot{P} = \omega_c p - \omega_c P = \frac{3}{2}\omega_c(v_{od} i_{od} + v_{oq} i_{oq}) - \omega_c P \tag{3.23}$$

$$\dot{Q} = \omega_c q - \omega_c Q = \frac{3}{2}\omega_c(v_{oq} i_{od} - v_{od} i_{oq}) - \omega_c Q \tag{3.24}$$

The nominal frequency and regular voltage together with the power measured before determine the reference power. The error between the measured power and the reference power is sent through a proportional-integral (PI) controller to obtain the current reference signal which will be used in the inner loop current controller. The droop equations

$$P_{cm} = P^* - \frac{1}{m}(\omega_{PLL} - \omega_n) \tag{3.25}$$

$$Q_{cm} = Q^* - \frac{1}{n}(v_{oq} - V_n) \tag{3.26}$$

The error between the power command and calculated power is sent to the outer controller to generate voltage command for the inner loop control.

$$\dot{\phi}_P = P - P^* \tag{3.27}$$

$$i_{ld,cm} = k_{ic}\phi_P + k_{pc}\dot{\phi}_P \tag{3.28}$$

$$\dot{\phi}_Q = Q^* - Q \tag{3.29}$$

$$i_{lq,cm} = k_{ic}\phi_Q + k_{pc}\dot{\phi}_Q \tag{3.30}$$

3.1.3.3. Inner control loop. This reference current is then compared with the current measured from the output terminal of the inverter which is before the LCL filter. The compared error is sent to the inner loop voltage controller to generate the final switching signals for the power electronics device of the converter. The inner loop equations are

$$\dot{\gamma}_d = i_{ld,cm} - i_{ld} \tag{3.31}$$

$$v_{ld,cm} = k_{iv}\gamma_d + k_{pv}\dot{\gamma}_d - \omega_n L_f i_{lq} \tag{3.32}$$

$$\dot{\gamma}_q = i_{lq,cm} - i_{lq} \tag{3.33}$$

$$v_{lq,cm} = k_{iv}\gamma_q + k_{pv}\dot{\gamma}_q + \omega_n L_f i_{ld} \tag{3.34}$$

3.1.3.4. LCL filter. The LCL filter has three components relative to differential equations, filter inductor L_f, coupling inductor L_c and filter capacitor C_f. All the resistance on the filter is lumped to R_d. The relative equations are

$$\dot{i}_{ld} = \frac{1}{L_f}(v_{id} - v_{od} - r_f i_{ld}) + \omega_{PLL} i_{lq} \tag{3.35}$$

$$\dot{i}_{lq} = \frac{1}{L_f}(v_{iq} - v_{oq} - r_f i_{lq}) - \omega_{PLL} i_{ld} \tag{3.36}$$

$$\dot{i}_{od} = \frac{1}{L_c}(v_{od} - v_{bd} - r_c i_{od}) + \omega_{PLL} i_{oq} \tag{3.37}$$

$$\dot{i}_{oq} = \frac{1}{L_c}(v_{oq} - v_{bq} - r_c i_{oq}) - \omega_{PLL} i_{od} \tag{3.38}$$

$$\dot{v}_{od} = \frac{1}{C_f}(i_{ld} - i_{od}) + \omega_{PLL} v_{oq} + R_d(\dot{i}_{ld} - \dot{i}_{od}) \tag{3.39}$$

$$\dot{v}_{oq} = \frac{1}{C_f}(i_{lq} - i_{oq}) - \omega_{PLL} v_{od} + R_d(\dot{i}_{lq} - \dot{i}_{oq}) \tag{3.40}$$

3.1.3.5. Local and global reference frames transformation. Every inverter has its own local reference frame. The variables derived from the local calculation cannot be use in the global reference frame directly. Every subsystems should be combined within a common reference frame which means a local-global transformation is needed. To achieve this, we choose one subsystem SST_1 as the global reference. Every other subsystem has a difference of rotation angle δ from the reference frame. So, the rotation transformation is

$$\begin{bmatrix} f_D \\ f_Q \end{bmatrix} = \boldsymbol{T}(\delta) \begin{bmatrix} f_d \\ f_q \end{bmatrix}, \quad \begin{bmatrix} f_d \\ f_q \end{bmatrix} = \boldsymbol{T}^{-1}(\delta) \begin{bmatrix} f_D \\ f_Q \end{bmatrix} \tag{3.41}$$

$$\boldsymbol{T}(\delta) = \begin{bmatrix} \cos\delta & \sin\delta \\ -\sin\delta & \cos\delta \end{bmatrix} \tag{3.42}$$

In (3.41) and (3.42), $\boldsymbol{T}(\delta)$ represents the rotation for angle δ anticlockwise. The variables with upper case subscripts DQ indicate the global reference frame, and the ones with lower case subscripts dq represent the local reference frame.

As shown in Fig. 3.1, every SST bus has a local constant impedance load on it, and every bus, including the bus with generator, is connected to 2 of its adjacent bus through transmission lines. The load at bus i is given by

$$\dot{i}_{lineD,ij} = \frac{1}{L_{line}}(v_{bD,i} - v_{bD,j} - r_{line}i_{lineD,ij}) + \omega_{PLL}i_{lineQ,ij} \tag{3.43}$$

$$\dot{i}_{lineQ,ij} = \frac{1}{L_{line}}(v_{bQ,i} - v_{bQ,j} - r_{line}i_{lineQ,ij}) - \omega_{PLL}i_{lineD,ij} \tag{3.44}$$

$i_{lineD,ij}$ means the current flow from bus i to bus j and so on.

3.1.3.6. Combination and evaluation of the mathematical model. Since the microgrid system is an islanded system, there is no grid frequency as reference, measured frequency of the first inverter can be set as the reference. But in this case, the global frequency ω_n is set as the reference frequency for the whole system. We notice that the phase angle δ equation (3.6) in section 3.1.2 will become

$$\dot{\delta} = \omega_n - \omega_{PLL}. \tag{3.45}$$

The phase angle derivations for DER_i will be

$$\dot{\delta} = \omega_n - \omega_{PLL,i}. \tag{3.46}$$

On every bus, the bus voltage and injected currents are related by virtual resistor equation (3.48). This method assumes a certain large resistance r_n between the bus and ground.

$$v_{bDQ,i} = r_n(i_{oDQ,i} - i_{loadDQ,i} + \sum_{j \neq i} i_{lineDQ,ji}) \tag{3.47}$$

$$i_{lineDQ,ji} = -i_{lineDQ,ij} \tag{3.48}$$

3.2. LINEARIZED MODEL

The system states are divided into 8 groups. The generator 1 and 2 both have 5 states. Each inverter out of 5 has 15 states. The loads have 14 states. The distribution lines have 14 states. There are 2 states for PI controller for the generators. Totally, there are 115 states.

$$\begin{aligned} x_{inv,i} = [&\delta_i \quad P_i \quad Q_i \quad v_{od,f,i} \quad \phi_{PLLi} \quad \phi_{Pi} \quad \phi_{Qi} \quad \gamma_{di} \quad \gamma_{qi} \\ &i_{ldi} \quad i_{lqi} \quad v_{odi} \quad v_{oqi} \quad i_{odi} \quad i_{oqi}] \qquad (1 \leqslant i \leqslant 5) \end{aligned} \tag{3.49}$$

$$x_{gen,6} = [\delta_6 \quad E_{f6} \quad \omega_6 \quad i_{D6} \quad i_{Q6}] \tag{3.50}$$

$$x_{gen,7} = [\delta_7 \quad E_{f7} \quad \omega_7 \quad i_{D7} \quad i_{Q7}] \tag{3.51}$$

$$x_{load,i} = [i_{loadD,i} \quad i_{loadQ,i}] \qquad (1 \leqslant i \leqslant 7) \tag{3.52}$$

$$x_{line,ij} = [i_{lineD,ij} \quad i_{lineQ,ij}] \qquad (i < j) \tag{3.53}$$

The state vector for all the system states is

$$x = [x_{inv,1} \cdots x_{inv,5} \quad x_{gen,6} \quad x_{gen,7} \quad i_{load,1} \cdots i_{load,7} \tag{3.54}$$

$$i_{line,12} \quad i_{line,23} \quad i_{line,37} \quad i_{line,47} \quad i_{line,45} \quad i_{line,56} \quad i_{line,16}] \tag{3.55}$$

The system equations can be described as

$$\dot{x} = f_{sys}(x) \tag{3.56}$$

The system A matrix can be derived by calculating the Jacobian derivation of equations group (3.56). The steady-state operating point of the microgrid x_{op} is the equilibrium solution of the nonlinear equations of the system. It can be derived by solving the following equations

$$0 = f_{sys}(x_{op}) \tag{3.57}$$

3.3. PROPOSED METHOD AND CORRESPOND CALCULATION

The 7-node microgrid system model is represented in the former chapter. At this point, the corresponding method for driving the system stable will be applied in the microgrid system.

3.3.1. Lyapunov Function Calculation. The microgrid system matrix A_{sys} can be calculated using the method from the previous chapter. The matrix P is generated by Lyapunov equation, and Lyapunov function comes out to be

$$V(\tilde{x}) = \tilde{x}^T P \tilde{x} \tag{3.58}$$

Because the high-order system transient cannot be plotted, the scalar Lyapunov function can be used to illustrate the change process during the switching actions.

3.3.2. State-Based Switching Condition. The switching condition equation (from mode 2 to mode 1) also holds the same form as the (2.31). It can be further simplified to (3.59)

$$\begin{aligned} \tilde{x}_1^T(P_1 + P_1^T)A_2\tilde{x}_2 &= 0 \\ M_{2,1} &= (P_1 + P_1^T)A_2 \\ \Rightarrow\ \tilde{x}_1^T M_{2,1}\tilde{x}_2 &= 0 \end{aligned} \tag{3.59}$$

4. SUMMARY AND CONCLUSIONS

The microgrid system is able to be destabilized by switching even if all individual subsystems are stable. The state-dependent best-case switching strategy described in this paper works for making a complicated seven-node microgrid system return stable operating points faster after a instant load change or power command change.

The microgrid system model in this thesis is relatively vulnerable so that it can be made unstable easily with the change of parameters in the system like droop equations and PI controller parameters. The method to guarantee stability will be even more important.

Lyapunov function based analysis is used to represent the system operating condition from a simple but direct way. And we can stabilize the microgrid system without dig into every subsystem's working condition but focus on the overall instability so that we can make switching at proper times to increase the system stability.

APPENDIX A

MATHEMATICA CODE OF THE MODEL

```
Clear["Global`*"];
```

This derives an average model of a normal boost converter circuit without control components.

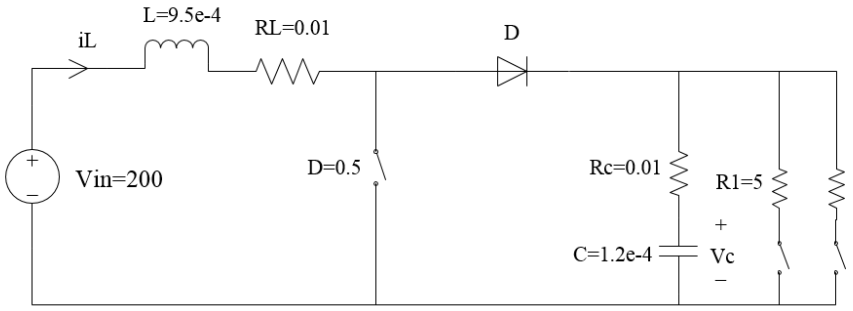

Switch Close Mode

(*

Close mode differential equations:

$i_L' == \frac{-R_L}{L} i_L + \frac{V_{in}}{L}$; $v_C' == \frac{-1}{(R_c+R)C} v_C$;

*)

$$dx11 = \frac{-Rl}{L}\, x11 + \frac{Vin}{L};$$

$$dx12 = \frac{-1}{(Rc + R)\ c}\, x12;$$

```
A1 = D[{dx11, dx12}, {{x11, x12}}];
MatrixForm[%]
```

$$\begin{pmatrix} -\frac{Rl}{L} & 0 \\ 0 & -\frac{1}{c\,(R+Rc)} \end{pmatrix}$$

```
B1 = D[{{dx11}, {dx12}} - A1.{{x11}, {x12}}, Vin];
MatrixForm[%]
```

$$\begin{pmatrix} \frac{1}{L} \\ 0 \end{pmatrix}$$

Switch Open Mode

State-space model calculation.

7-Bus Microgrid System Model

```
Clear["Global`*"];
```

Parameters

```
(* Substitution *)
    {wc, wn, wcPLL, m, n,
       kpPLL, kiPLL, kppq, kipq, kim, kpm,                          kicd, kicq, kpcd, kp
       Lf, Lc, Cf, Rd,                                rf, rc, Lline, rline, rn,
       Rload01, Rload02, Lload01, Lload02, Rpert, Lpert, Rload, Lload,

       H, Xt, Xd, Xq, Xdp, Tmc, Rmc, Trate(*Transformer's rate*),
       Ka, Ta, Td0p} =


      {50.26, 377.0, 7853.98, 0.001, 0.001,
       0.25, 2.0, 0.0005, 0.025, 25, 0.25,                                  100.0, 100.0
       4.2 * 10^-3, 0.5 * 10^-3, 15.0 * 10^-6, 2.025,      0.5, 0.09, 1.97 * 10^-3, 0.77,
       25, 25, 15 * 10^-3, 7.5 * 10^-3, 25, 7.5 * 10^-3, , 25, 7.5 * 10^-3,

       (*0.025*)2.586, 0.0067, 0.6534, 0.3364, 0.04, (* *)0.03, (*0.49,*)0.001, (* *)1,
       180, 0.02, 5.48};


    {Pstar01, Qstar01, Pstar02, Qstar02, Vstar} = {-50 000, 0, 50 000, 0, 12 470};

    {Vref, Pref} = {Vstar / Trate, 381 000};(* SST:285kVA  droop Gen:400kW 5%*)

(*    delta01=0;*)
```

Line current conversion;

7-node microgrid system model.

APPENDIX B

MATLAB CODE FOR SWITCHING

```
format compact
% A1=subs(A1,[R d L c Rc Rl Vin] , [3. 0.5 9.5/10^4 1.2/10^4 0.01 0.01 200]);
% A2=subs(A2,[R2 d L c Rc Rl Vin] , [5. 0.5 9.5/10^4 1.2/10^4 0.01 0.01 200]);
% A3=subs(A2,[R3 d L c Rc Rl Vin] , [1.875 0.5 9.5/10^4 1.2/10^4 0.01 0.01 200]);
% A4=subs(A2,[R3 d L c Rc Rl Vin] , [1. 0.5 9.5/10^4 1.2/10^4 0.01 0.01 200]);

    R=[1.875, 500, 30, 8, 4];
%     R=[1.875, 100, 10, 8, 4];
%     R=[1.875, 90, 10, 8, 4];
%     R=[1.875, 1500, 40, 8, 4];
%     d=0.5;
    d=0.1;
    L=9.5/10^4;
    c=1.2/10^4;
    Rc=0.01;
    Rl=0.01;
    Vin=200;

A1=[(R(1)*((-1 + d)*Rc - Rl) - Rc*Rl)/(L*(R(1) + Rc)),((-1 + d)*R(1))/(L*(R(1) + Rc));(R
(1) - d*R(1))/(c*R(1) + c*Rc),-(1/(c*R(1) + c*Rc))];
A2=[(R(2)*((-1 + d)*Rc - Rl) - Rc*Rl)/(L*(R(2) + Rc)),((-1 + d)*R(2))/(L*(R(2) + Rc));(R
(2) - d*R(2))/(c*R(2) + c*Rc),-(1/(c*R(2) + c*Rc))];
A3=[(R(3)*((-1 + d)*Rc - Rl) - Rc*Rl)/(L*(R(3) + Rc)),((-1 + d)*R(3))/(L*(R(3) + Rc));(R
(3) - d*R(3))/(c*R(3) + c*Rc),-(1/(c*R(3) + c*Rc))];
% P=[0.0199147,-0.000044551;-0.000044551,0.00251315];
% [50;395]
% X:[3; 5;  1.875;  1;  4];
% L c still use 10^4, Rc Rl still use 0.01.
% X1=[262.298;393.447];3
% X2=[158.416;396.041];5
% X3=[415.596,389.621];1.875
% % X4=[761.977;380.988];1
% % X4=[79.6021;398.01];10
% X4=[99.379;397.516];8
% X5=[197.532;395.064];4

% X:[3000,5000,1875,8000,4000];

% X1=[19.975,399.501];
% X2=[9.99375,399.75];
% X3=[42.5532,398.936];
% X4=[158.416;396.041];
% X5=[262.298;393.447];
% X1=[1.9975,399.501];
% X2=[0.999375,399.75];
% X3=[4.25532,398.936];
% X4=[1.5984,399.6];
% X5=[2.66223,399.334];
% {19.7532,395.064}
% {9.9379,397.516}
% {41.5596,389.621}
```

Operating point set up.

11/29/17 11:58 AM Block: Boost_2ss_Apr10_50.../ Functions1 1 of 2

```
function [flag1,at2,at3,abs23,abs32,cmpr23,cmpr32,fl1,fl2] = SwitchCondition(xpre2,xpre3,
xaft,xx1,xx2,xx1dl,xx2dl)
%#codegen
cond3to2 = -159971. + 21.3162*xx1 - 1.00059*xx1^2 + 4423.36*xx2 - 0.209085*xx1*xx2 -
10.0588*xx2^2;
cond2to3 = -160177. + 51.2502*xx1 - 1.00021*xx1^2 + 399.672*xx2 - 0.0325521*xx1*xx2 +
0.00165803*xx2^2;

% [100 10]
% -159904. + 33.0105*xx1 - 0.999952*xx1^2 + 4203.67*xx2 - 0.0755656*xx1*xx2 - 9.51376
*xx2^2;
% -164749. + 157.289*xx1 - 1.0008*xx1^2 + 412.585*xx2 - 0.149376*xx1*xx2 - 0.00574871
*xx2^2;
% [500 30]
% -159971. + 21.3162*xx1 - 1.00059*xx1^2 + 4423.36*xx2 - 0.209085*xx1*xx2 - 10.0588
*xx2^2;
% -160177. + 51.2502*xx1 - 1.00021*xx1^2 + 399.672*xx2 - 0.0325521*xx1*xx2 + 0.00165803
*xx2^2;
% [10 5]
% -164749. + 161.328*xx1 - 0.999116*xx1^2 + 1221.25*xx2 + 0.165658*xx1*xx2 - 2.10263
*xx2^2;
% -181944. + 315.879*xx1 - 1.00094*xx1^2 + 600.746*xx2 - 0.181249*xx1*xx2 - 0.443264
*xx2^2;
% [50 5]
% -159936. + 50.4173*xx1 - 0.999128*xx1^2 + 4489.77*xx2 + 0.0819328*xx1*xx2 - 10.2408
*xx2^2;
% -181944. + 315.114*xx1 - 1.00169*xx1^2 + 447.401*xx2 - 0.32651*xx1*xx2 + 0.00292
*xx2^2;
% [50 30]
% -706960 + 122.672*xx1 - 0.999838*xx1^2 + 2845.54*xx2 + 0.015195*xx1*xx2 - 2.71376
*xx2^2;
% 57507.5 + 17.0612*xx1 - 1.00026*xx1^2 - 15.1487*xx2 - 0.0461341*xx1*xx2 - 0.320493
*xx2^2;
% [40 5]
% -160000. + 54.539*xx1 - 0.998986*xx1^2 + 3717.49*xx2 + 0.129683*xx1*xx2 - 8.31364
*xx2^2;
% -181944. + 315.161*xx1 - 1.00164*xx1^2 + 456.992*xx2 - 0.317424*xx1*xx2 - 0.0249808
*xx2^2;
at2 = ~any(xpre2-xaft);% Ture only if xpre2==xaft
at3 = ~any(xpre3-xaft);
abs23 = abs(cond2to3);
abs32 = abs(cond3to2);
cmpr23 = abs23<=3000;
cmpr32 = abs32<=3000;
persistent flag;           % Used for controlling the switch
if isempty(flag)
    flag=1;
else
end

persistent f1;             % Used for judging that if the switching condition equation
```

Switching map control.

REFERENCES

[1] D. Baimel, J. Belikov, J. M. Guerrero, and Y. Levron. Dynamic modeling of networks, microgrids, and renewable sources in the dq0 reference frame: A survey. *IEEE Access*, 5:21323–21335, 2017.

[2] J. Belikovab and Y. Levronc. Comparison of time-varying phasor and dq0 dynamic models for large transmission networks. *2017 International Journal of Electrical Power and Energy Systems*, pages 65–74, Dec 2017.

[3] H. Bosetti and S. Khan. Transient stability in oscillating multi-machine systems using lyapunov vectors. *IEEE Transactions on Power Systems*, PP(99):1–1, 2017.

[4] M. S. Branicky. Multiple lyapunov functions and other analysis tools for switched and hybrid systems. *IEEE Transactions on Automatic Control*, 43(4):475–482, Apr 1998.

[5] J. Daafouz, P. Riedinger, and C. Iung. Stability analysis and control synthesis for switched systems: a switched lyapunov function approach. *IEEE Transactions on Automatic Control*, 47(11):1883–1887, Nov 2002.

[6] L. Galotto, C. A. Canesin, R. Cordero, C. A. Quevedo, and R. Gazineu. Non-linear controller applied to boost dc-dc converters using the state space average model. In *2009 Brazilian Power Electronics Conference*, pages 733–740, Sept 2009.

[7] C. Yang H. Ma and Y. Zhang. Analysis and design for single-phase three-level boost pfc converter with quasi-static model. In *IECON 2011 - 37th Annual Conference of the IEEE Industrial Electronics Society*, pages 4385–4390, Nov 2009.

[8] A. Q. Huang. Medium-voltage solid-state transformer: Technology for a smarter and resilient grid. *IEEE Industrial Electronics Magazine*, 10(3):29–42, Sept 2016.

[9] B. B. Johnson, A. Davoudi, P. L. Chapman, and P. Sauer. Microgrid dynamics characterization using the automated state model generation algorithm. In *Proceedings of 2010 IEEE International Symposium on Circuits and Systems*, pages 2758–2761, May 2010.

[10] G. G. Karady, A. Q. Huang, and M. Baran. Freedm system: An electronic smart distribution grid for the future. In *PES T D 2012*, pages 1–6, May 2012.

[11] R. H. Lasseter and P. Paigi. Microgrid: a conceptual solution. In *2004 IEEE 35th Annual Power Electronics Specialists Conference (IEEE Cat. No.04CH37551)*, volume 6, pages 4285–4290 Vol.6, June 2004.

[12] Z. Li, Y. Yang, and X. Bao. Simulation and analysis of the third-order model of synchronous generator based on mfc. In *2009 International Conference on Mechatronics and Automation*, pages 4252–4256, Aug 2009.

[13] D. Liberzon. *Switching in Systems and Control*. Birkhauser, Boston, 2003.

[14] D. Liberzon and A. S. Morse. Basic problems in stability and design of switched systems. *IEEE Control Systems*, 19(5):59–70, Oct 1999.

[15] J. A. Mueller and J. W. Kimball. Generalized average modeling of dc subsystem in solid state transformers. In *2017 IEEE Energy Conversion Congress and Exposition (ECCE)*, pages 1659–1666, Oct 2017.

[16] Y. Ni, S. Chen, and B. Zhang. *Theory and Analysis of Dynamic Power Systems*. Tsinghua University Press, 2002.

[17] T. Paul. *APPLICATION OF UNIFIED INVARIANTS FOR CYBER PHYSICAL SYSTEMS IN SMART GRIDS*. Ph.d. dissertation, Missouri University of Science and Technology, 2015.

[18] M. Rasheduzzaman, J. Mueller, and J. W. Kimball. Small-signal modeling of a three-phase isolated inverter with both voltage and frequency droop control. In *2014 IEEE Applied Power Electronics Conference and Exposition - APEC 2014*, pages 1008–1015, Mar 2014.

[19] M. Rasheduzzaman, J. A. Mueller, and J. W. Kimball. An accurate small-signal model of inverter- dominated islanded microgrids using *dq* reference frame. *IEEE Journal of Emerging and Selected Topics in Power Electronics*, 2(4):1070–1080, Dec 2014.

[20] R. H. G. Tan and L. Y. H. Hoo. Dc-dc converter modeling and simulation using state space approach. In *2015 IEEE Conference on Energy Conversion (CENCON)*, pages 42–47, Oct 2015.

[21] T. L. Vandoorn, J. C. Vasquez, J. De Kooning, J. M. Guerrero, and L. Vandevelde. Microgrids: Hierarchical control and an overview of the control and reserve management strategies. *IEEE Industrial Electronics Magazine*, 7(4):42–55, Dec 2013.

[22] N. Wang, H. Liu, and W. Chen. Lyapunov-based excitation control for the synchronous generator unit. In *Proceedings of the 32nd Chinese Control Conference*, pages 899–903, July 2013.

VITA

Bokang Zhou received his Bachelor's degree in Electrical Engineering from Beijing Jiaotong University, China in 2015. He received his M.S. degree from Missouri University of Science and Technology (Missouri S&T), Rolla, MO, USA, in Electrical Engineering in May 2018. His research interests included design, control and stability analysis of microgrid systems.